

広島大学学術情報リポジトリ
Hiroshima University Institutional Repository

Title	Fulde-Ferrell-Larkin-Ovchinnikov State in Quasi-One-Dimensional Systems: Correlation between Fermi-Surface Distortion and Optimal In-Plane Magnetic-Field Direction
Author(s)	Itahashi, Katsumi; Shimahara, Hiroshi
Citation	Journal of the Physical Society of Japan , 89 : 024708-1 - 024708-8
Issue Date	2020-01-29
DOI	10.7566/JPSJ.89.024708
Self DOI	
URL	https://ir.lib.hiroshima-u.ac.jp/00051553
Right	Copyright (c) 2020 The Physical Society of Japan This is not the published version. Please cite only the published version. この論文は出版社版ではありません。引用の際には出版社版をご確認、ご利用ください。
Relation	



Fulde–Ferrell–Larkin–Ovchinnikov State in Quasi-One-Dimensional Systems: Correlation Between Fermi-Surface Distortion and Optimal In-Plane Magnetic-Field Direction

Katsumi Itahashi* and Hiroshi Shimahara†

*Department of Quantum Matter Science, ADSM, Hiroshima University,
Higashi-Hiroshima, Hiroshima 739-8530, Japan*

(Received October 7, 2019)

The Fulde–Ferrell–Larkin–Ovchinnikov (FFLO) state is systematically examined in a generic model of quasi-one-dimensional (Q1D) type-II superconductors that has six hopping integrals of electrons as model parameters. For a magnetic field parallel to the conductive layers, the upper critical field H_{c2} is strongly enhanced by the FFLO state at low temperatures and sensitively depends on the angle ϕ between the in-plane magnetic field and the highly conductive chain (the crystal a-axis). As a result, H_{c2} exhibits sharp peaks at the optimal angles $\phi = \pm\phi_0$. Since the optimal angle ϕ_0 strongly depends on the structure of the Fermi surface, we examine their correlation, searching for an intuitive method to find ϕ_0 from the shape of the Fermi surface. For this purpose, we define quantities that quantify the warp of each sheet ($k_x > 0$ or $k_x < 0$) of the Q1D open Fermi surface and the shear distortion between the two sheets. We estimate the optimal angles for numbers of the parameter sets chosen systematically from a large area of the parameter space. It is found that in most cases, the optimal direction of the in-plane magnetic field tends to be roughly parallel to the a-axis. This result, together with the fact that the orbital pair-breaking effect is weakest for $\phi = 0$, implies that the FFLO state is most stabilized for a small ϕ . However, when the warp is small while the shear distortion is moderate, the FFLO state can be maximally stabilized for any in-plane magnetic-field direction except for the directions between the b- and b'-axes, where the b'-axis is perpendicular to the a-axis. The phase diagrams of the optimal angle and the upper critical field at zero temperature are also presented. A jump of the optimal angle ϕ_0 when the pressure varies is predicted.

1. Introduction

In quasi-low-dimensional type-II superconductors, the existence of the Fulde–Ferrell–Larkin–Ovchinnikov (FFLO) state^{1,2)} has been suggested.^{3–19)} The FFLO state can be stabilized when the magnetic field is oriented parallel to the highly conductive layers because such an orientation suppresses the orbital pair-breaking effect.^{20–22)} In the FFLO state in such systems, dependences of the upper critical field H_{c2} and the transition temperature T_c on the direction of the in-plane magnetic field must be quite different²³⁾ from those in the conventional BCS state because of the nonzero center-of-mass momentum \mathbf{q} of the Cooper pairs,²⁴⁾ which is a characteristic of the FFLO state. Therefore, they can be direct evidence for the FFLO state, if they are experimentally observed and theoretically reproduced.

For example, in the quasi-one-dimensional (Q1D) organic superconductor $(\text{TMTSF})_2\text{ClO}_4$, the observed onset temperature of superconductivity $T_c^{\text{onset}}(\phi)$ exhibits an exotic field-angle dependence at high fields,^{13–15)} which is quite different from that expected for the conventional BCS state. Here, TMTSF stands for tetramethyltetraselenafulvalene, and ϕ denotes the angle between the in-plane magnetic field and the crystal a-axis. From this fact and other circumstantial evidence, the possibility of the FFLO state has been examined by some authors as explained below.

In Q1D systems in which the Fermi velocity is approximately parallel to the a-axis everywhere on the Fermi surface, the strength of the orbital pair-breaking effect on the BCS state is principally determined by the magnetic-field compo-

nents perpendicular to the a-axis. In fact, in the polar plot of $T_c^{\text{onset}}(\phi)$ observed in $(\text{TMTSF})_2\text{ClO}_4$ at low fields, the principal axes are parallel to the a-axis and the b'-axis, where the b'-axis is perpendicular to the a-axis. Hence, the orbital pair-breaking effect is considered to dominate the ϕ dependence of T_c^{onset} . At high fields, however, the latter principal axis deviates from the b'-axis,^{13–15)} which suggests the emergence of an exotic high-field superconducting phase. The FFLO state is considered to be a plausible candidate for this high-field phase^{13–15,25–28)} because of the following circumstantial evidence: (1) the quasi-low-dimensionality and narrow energy band are advantageous to the FFLO state,^{4–7)} and (2) the upper critical field $H_{c2}(T)$ exhibits upturn,^{12,15)} which is consistent with that in the FFLO state.^{6,25)}

Although the accurate theoretical reproduction of $T_c(\phi)$ is desirable, it is difficult in practice because accurate information for the electron dispersion, to which the FFLO state is sensitive, is unavailable at present. However, it was shown by a theory explained below²⁶⁾ that parameter values in a range realistic for $(\text{TMTSF})_2\text{ClO}_4$ can reproduce the observed direction of the exotic principal axis.

The field-angle dependence characteristic of the FFLO state principally originates from the direction of the FFLO vector \mathbf{q} relative to the anisotropic Fermi surface. In the FFLO state, since the direction of \mathbf{q} is locked in the direction of the magnetic field \mathbf{H} unless the orbital pair-breaking effect is extremely weak,^{5,20,21,29,30)} we obtain $\phi_{\mathbf{q}} = \pm\phi$, where $\phi_{\mathbf{q}}$ denotes the angle between \mathbf{q} and the a-axis. Hence, the dependence of H_{c2} on the field direction is equivalent to that on the direction of \mathbf{q} . For each fixed $\phi_{\mathbf{q}}$ ($= \phi$), the magnitude $q = |\mathbf{q}|$ is optimized so that the upper critical field is maximized and the free energy is minimized. The strong ϕ de-

*Present address: Center for Education and Innovation, Sojo University, 4-22-1 Ikeda, Nishi-ku, Kumamoto 860-0082, Japan

†Corresponding author. E-mail: hiro@hiroshima-u.ac.jp

pendence of $H_{c2}(\phi)$ is due to the Fermi-surface effect called the nesting effect for the FFLO state,^{6,7,31,32} which is analogous to the nesting effect for the spin- and charge-density waves (SDW and CDW, respectively). The optimal angle ϕ_0 that maximizes $H_{c2}(\phi)$ is principally determined by the structure of the Fermi surface, although the orbital pair-breaking effect may modify it.

In our previous study,²⁶ we examined the upper critical field in a model of the Q1D systems in which the inter-layer electron motion is negligible, and we found sharp peaks (cusps) in $H_{c2}(\phi)$ at particular angles $\phi = \pm\phi^{\text{cusp}}$, which implies that $\phi_0 = \phi^{\text{cusp}}$ in this case. The cusps originate from the FFLO state, and the magnitudes of $H_{c2}(\phi)$ for $\phi \approx \pm\phi^{\text{cusp}}$ exceed five times the Pauli paramagnetic limit H_P . Such large values imply that the FFLO state is strongly stabilized for $\phi \approx \pm\phi^{\text{cusp}}$, although the value of the upper critical field must be reduced by the orbital pair-breaking effect induced by inter-layer electron motion, which occurs in the real compounds. The cusp angle ϕ^{cusp} is determined by the Fermi-surface effect mentioned above.

After the above study, we were interested in determining whether the obtained optimal directions are common in Q1D systems and whether a similar dependence on ϕ would be likely observed in future experiments on Q1D compounds. Hence, in this paper, we examine the correlation between the optimal field direction and the structure of the Fermi surface. We focus on the distortion of the sheets of the open Fermi surfaces in Q1D superconductors that is characterized by the warp of each sheet and the shear distortion between the two sheets. We search for an intuitive method to predict ϕ_0 from the shape of the Fermi surface, examining ϕ_0 for parameter values chosen systematically from a broad range. The results would be useful because the shape of the Fermi surface can be provided by first-principles calculations for candidate compounds for the FFLO state.

In Sec. 2, we briefly review the nesting effect and the origin of the cusps to clarify the purpose of the present study. In Sec. 3, we define our model of electron dispersion, which contains six hopping integrals. We define parameters k_w and k_s that characterize the warp and the shear distortion of the Fermi surface, respectively. In Sec. 4, we present numerical results. The optimal angle ϕ_0 and the upper critical field $H_{c2}(\phi_0)$ as functions of the hopping integrals are examined in detail. We obtain phase diagrams and correlation maps, which clarify the dependences of ϕ_0 and $H_{c2}(\phi_0)$ on the electron dispersion and the distortion of the Q1D Fermi surface. In the final section, we summarize the results.

2. Nesting Effect and Origin of Cusps

The distortion of the Fermi surface plays essential roles in the FFLO state. First, a sufficient distortion of the Fermi surface from the flat shape is indispensable for the emergence of the FFLO state in Q1D systems because, otherwise, the SDW or CDW transition would occur at a low temperature. Furthermore, when the distortion is sufficiently large for the transitions to SDW and CDW to be suppressed, the resultant two-dimensional system can be a good candidate for an FFLO superconductor because of the nesting effect for the FFLO state.^{6,7,31,32} The resultant $H_{c2}(T)$ does not diverge in the limit $T \rightarrow 0$, in contrast to the purely one-dimensional system, and $dH_{c2}(T)/dT$ does not vanish in the same limit,

in contrast to the isotropic three-dimensional system. In this context, Q1D organic superconductors with sufficiently large distortion of the Fermi surfaces that suppresses SDW and CDW, such as $(\text{TMTSF})_2\text{ClO}_4$, should be classified as a quasi-two-dimensional superconductor.⁶ In such systems, $H_{c2}(T)$ can exhibit a dimensional crossover from the purely one-dimensional to the quasi-two-dimensional systems as the temperature T decreases.²⁵

The nesting effect for the FFLO state cannot be predicted from simple consideration based only on the shape of the Fermi surface.^{31,32} For example, it may be speculated from analogy with the one-dimensional FFLO superconductors^{33,34} that a nearly flat portion of the Fermi surface can strongly enhance the critical field, with \mathbf{q} becoming perpendicular to the nearly flat portion. However, these speculations fail, as elucidated by detailed calculations in the previous studies.^{7,26,31,32}

This difficulty is due to the fact that the nesting effect for the FFLO state concerns not only the shape of the Fermi surface but also derivatives of the one-particle energy $\epsilon(\mathbf{k})$ of the electrons on the Fermi surface, such as the Fermi velocity. To explain this fact, we defined the difference Δk_{Fx} of the Fermi surfaces in our previous papers.^{26,32} Let us refer to the one-particle energy of the electrons as $\xi_\sigma(\mathbf{k}, h) \equiv \epsilon(\mathbf{k}) - \sigma h - \mu$, where μ is the chemical potential and $h = \mu_e |\mathbf{H}|$ with the electron magnetic moment μ_e and the magnetic field \mathbf{H} . The Fermi surfaces are expressed by $k_x = k_{\text{Fx}}^\sigma(k_y, h)$, where $\xi_\sigma(k_{\text{Fx}}^\sigma(k_y, h), k_y, h) = 0$ for $\sigma = \uparrow$ and \downarrow . Because the FFLO state is induced by the pairing of electrons with (\mathbf{k}, \uparrow) and $(-\mathbf{k} + \mathbf{q}, \downarrow)$, we consider the difference

$$\Delta k_{\text{Fx}}(k_y, \mathbf{q}, h) \equiv k_{\text{Fx}}^\downarrow(k_y - q_y, h) - k_{\text{Fx}}^\uparrow(k_y, h) + q_x \quad (1)$$

between the Fermi surface of up-spin electrons and that of down-spin electrons shifted by \mathbf{q} . This function is expanded as

$$\Delta k_{\text{Fx}}(k_y, \mathbf{q}, h) = \sum_{k=n}^{\infty} c_k(\mathbf{q}, h) [k_y - k_y^0(\mathbf{q}, h)]^k \quad (2)$$

near $k_y = k_y^0(\mathbf{q}, h)$, which is defined by $\Delta k_{\text{Fx}}(k_y^0(\mathbf{q}, h), \mathbf{q}, h) = 0$, where $n \geq 1$ and $c_n \neq 0$. When $n = 1$, the Fermi surfaces cross each other as shown in Fig. 1(a), and H_{c2} is not strongly enhanced by the FFLO state. However, when $n \geq 2$, they touch each other as shown in Fig. 1(b) – (d), and thus, the upper critical field is strongly enhanced. In general, for a larger n , $\Delta k_{\text{Fx}}(k_y, \mathbf{q}, h)$ is smaller near $k_y = k_y^0$, and thus, the upper critical field is more strongly enhanced because electron pairs having small Δk_{Fx} substantially contribute to the FFLO state. Note that in Fig. 1, the difference between the Fermi surfaces of up- and down-spin electrons is magnified for clarity. In actuality, because usually $h \sim \mu_e H_P \sim \Delta_0 \ll W$ and we take the limit $\Delta_0/W \rightarrow 0$ in the weak coupling theory, the difference between the Fermi surfaces determined by $\xi_\sigma(\mathbf{k}, h) = 0$ and $\xi_\sigma(\mathbf{k}, 0) = 0$ is too small to be visible in the Brillouin zone, where Δ_0 and W are the zero-field gap and band width, respectively. (This is why we do not specify the magnitude of the magnetic field when we use the phrase “the shape of the Fermi surface.”)

It might be confusing that the equations $\xi_\sigma(\mathbf{k}, h) = 0$ determine the shapes of the Fermi surfaces at finite fields, and hence, the information contained in the shapes of the Fermi

surfaces might appear to be equivalent to that contained in the equations $\xi_\sigma(\mathbf{k}, h) = 0$, which lead to Eqs. (1) and (2). However, h in $\xi_\sigma(\mathbf{k}, h) = 0$ does not affect the (visible) shape of the Fermi surface, because $h \ll W$. In contrast, we cannot replace $\xi_\sigma(\mathbf{k}, h)$ with $\xi_\sigma(\mathbf{k}, 0)$ in the gap equation, even when $h \ll W$, because $h_c \sim \Delta_0$. Hence, the equations $\xi_\sigma(\mathbf{k}, h)$ contain more information than just the shape of the Fermi surface at zero field (or those at weak fields such that $h \ll W$). The derivatives of $\epsilon(\mathbf{k})$ on the Fermi surface cannot be obtained from the shape of the Fermi surface, because they depend not only on the values of $\epsilon(\mathbf{k})$ on the Fermi surface but also the values infinitesimally off the Fermi surface.

On the basis of the argument around Eqs. (1) and (2), the origin of the cusps can be generally explained as follows. Let us consider the upper critical field $H_{c2}(p)$ as a function of a certain parameter p , such as ϕ and the hole density n_h . It is verified by a geometric consideration that when q is optimized, $n = 2$ for almost all p in quasi-two-dimensional superconductors; however, at particular values of p , the factor c_2 for the optimal q can vanish, which means $n \geq 3$, and $H_{c2}(p)$ exhibits a cusp, as found in our previous papers.^{26,31)} We refer to such a value of p as p^{cusp} . In the square lattice system,^{31,32)} the structure of the Fermi surface changes when n_h changes, and thus, H_{c2} is a function of n_h . In this case, the cusp occurs in $H_{c2}(n_h)$ at the hole density $n_h^{\text{cusp}} = 0.630$, where $n = 4$, and H_{c2} exceeds five times H_p near $n_h = n_h^{\text{cusp}}$ because of the FFLO state. In the present Q1D system,²⁶⁾ the cusp occurs in $H_c(\phi)$ at particular angles $\pm\phi^{\text{cusp}}$, and H_{c2} is extremely enhanced near $\phi = \pm\phi^{\text{cusp}}$ as mentioned above. In contrast to the former case, $n = 3$ at $\phi = \pm\phi^{\text{cusp}}$ (Ref. 35). These phenomena are physically the same, except for the fact that the controlled parameters are different. Other possible examples of the controlled parameter p are a pressure, an electric field, and a doping ratio of a chemical element.

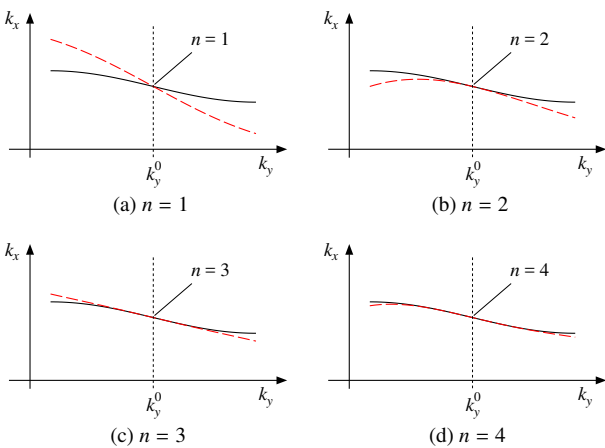


Fig. 1. Schematics that explain the intersections of the Fermi surfaces at $k_y = k_y^0$ with different values of n . The solid black and dashed red curves represent the Fermi surfaces of up-spin electrons and those of down-spin electrons shifted by q , respectively.

On the basis of the above argument, the purpose of the present study can be explained as follows. Equation (2) clarifies that both the shape of the Fermi surface and derivatives of $\xi(\mathbf{k})$ concern the nesting effect for the FFLO state. It is eas-

ily verified that the expression for ϕ^{cusp} contains the derivatives of $\xi(\mathbf{k})$ up to the third order. Hence, we cannot precisely predict the value of ϕ^{cusp} only from the shape of the Fermi surface. However, if there exists any intuitive method to approximately predict ϕ_0 , it would be convenient for practical use. We search for such a method in the following, examining ϕ_0 for many parameter sets chosen systematically so that a broad range of parameter sets is covered.

3. Model and Typical Theoretical Results

We examine a generic Q1D system having two intra-chain hopping integrals t_{S1} and t_{S2} and four inter-chain hopping integrals t_{I1} , t_{I2} , t_{I3} , and t_{I4} , which are depicted in Fig. 2. We consider this model because it includes an approximate model of $(\text{TMTSF})_2\text{ClO}_4$,^{26,36,37)} where the anion order^{38,39)} is ignored. When the molecules are dimerized, the sites A and B are inequivalent, and each pair of adjacent sites A and B constitutes a lattice site. For this lattice, we assume a half-filled hole band, which corresponds to a quarter-filled hole band when the sites A and B are equivalent.

For an explicit calculation of the optimal angle, we need to assume cell parameters.⁴⁰⁾ As an example, we adopt those for $(\text{TMTSF})_2\text{ClO}_4$,^{36,41)} i.e., $a = 7.083 \text{ \AA}$, $b = 7.667 \text{ \AA}$, $c = 13.182 \text{ \AA}$, $\alpha = 84.40^\circ$, $\beta = 87.62^\circ$, and $\gamma = 69.00^\circ$, where we halve the lattice constant b because the anion order is ignored.

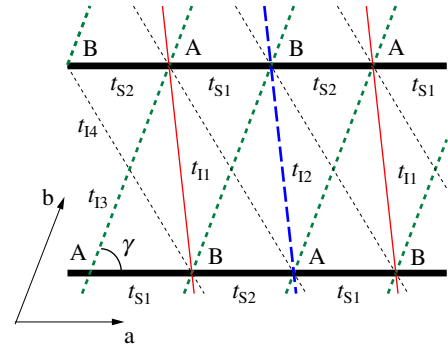


Fig. 2. Definitions of the hopping integrals presented in real space. The nodes labeled by A and B correspond to TMTSF molecules that are inequivalent in the unit cell. The hopping integrals between the sites A and B connected by the thick black solid lines are t_{S1} and t_{S2} . Those between the sites connected by the thin red solid, thick blue dashed, thick green short-dashed, and thin black dotted lines are t_{I1} , t_{I2} , t_{I3} , and t_{I4} , respectively. The angle γ and the lengths of the lines reflect the real lattice parameters of $(\text{TMTSF})_2\text{ClO}_4$ described in the text.

We define the components of the crystal momentum \mathbf{k} as $k_x = \mathbf{k} \cdot \mathbf{a}$, $k_y = \mathbf{k} \cdot \mathbf{b}$, and $k_z = \mathbf{k} \cdot \mathbf{c}$, where \mathbf{a} , \mathbf{b} , and \mathbf{c} are the lattice vectors along the crystal a -, b -, and c -axes, respectively. The electron dispersion relation is expressed as^{26,37,42)}

$$\epsilon(\mathbf{k}) = \epsilon_{AA}(\mathbf{k}) - \epsilon_{AB}(\mathbf{k}), \quad (3)$$

where

$$\begin{aligned} \epsilon_{AA}(\mathbf{k}) &= -2t_{I3} \cos k_y - 2t_{I4} \cos(k_x - k_y), \\ \epsilon_{AB}(\mathbf{k}) &= \sqrt{\epsilon_0^2 + [\epsilon_1(\mathbf{k})]^2}, \end{aligned} \quad (4)$$

and

$$\begin{aligned}\epsilon_0^2 &= t_{S1}^2 + t_{S2}^2 + t_{I1}^2 + t_{I2}^2, \\ \epsilon_1^2 &= 2t_{S1}t_{S2} \cos k_x + 2(t_{S1}t_{I1} + t_{S2}t_{I2}) \cos k_y \\ &\quad + 2(t_{S1}t_{I2} + t_{S2}t_{I1}) \cos(k_x - k_y) \\ &\quad + 2t_{I1}t_{I2} \cos(k_x - 2k_y).\end{aligned}\quad (5)$$

We assume the d-wave pairing interaction^{43–45)} presented in our previous letter,²⁶⁾ which induces the gap function of the form $\Delta(s, k_y) = \Delta_d \gamma_d(s, k_y)$, where $k_x = sk_{Fx}(k_y)$ and $\gamma_d(k_y) = \sqrt{2} \cos k_y$. The equation for the critical field is shown in the previous papers.^{25,26,31)} For each $\phi_q = \phi$, the magnitude $q = |\mathbf{q}|$ takes the value that maximizes the upper critical field.

Figure 3 shows the behaviors of $h_c(\phi) \equiv \mu_c H_{c2}(\phi)$ for samples of the parameter sets in which the cusps emerge. The zero-field gap Δ_{d0} is defined by $\Delta_{d0} = 2\omega_c \exp(-1/\lambda_d)$, where λ_d and ω_c denote the dimensionless coupling constant and the cut-off frequency, respectively. The Pauli paramagnetic limit is calculated by using the formula shown in Ref. 31. The profile of $H_{c2}(\phi)$ sensitively changes when the inter-chain hopping integrals vary. For example, the optimal direction can fall in any quadrant depending on the inter-chain integrals, whereas the maximum of $H_{c2}(\phi)$ tends to avoid the directions near the crystal b- and b'-axes. We examine these behaviors more systematically below.

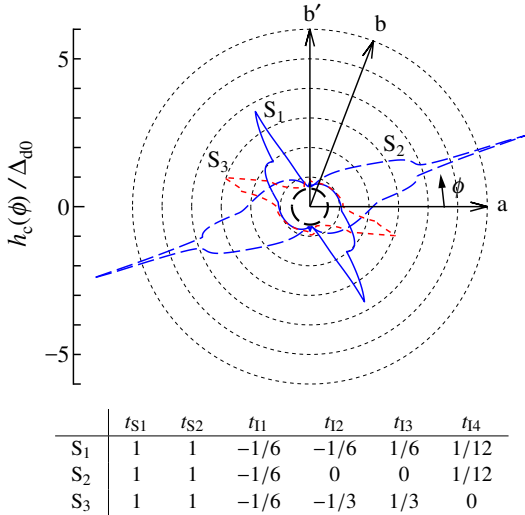


Fig. 3. Upper critical fields at $T = 0$. The blue solid, blue dashed, and red short-dashed curves show the results for the parameter sets S_1 , S_2 , and S_3 , respectively.

To examine the effect of the distortion of the Fermi surface, we define parameters that quantify the shape of the Fermi surface. The open Q1D Fermi surface consists of two sheets with $k_x > 0$ and $k_x < 0$, each of which is warped, and the two sheets are shifted in opposite directions along the k_y -axis, analogous to the shear distortion of continuum media. Hence, we consider two characteristics: the warp of each sheet and the shear distortion between the two sheets, the degrees of which are quantified by $k_w = k_x^t - k_x^b$ and $k_s = 2k_y^t$, respectively, where $(k_x^t, k_y^t) \equiv \mathbf{k}^t$ and $(k_x^b, k_y^b) \equiv \mathbf{k}^b$ are the top and bottom of the warped sheet with $k_x > 0$, respectively. These definitions are depicted in Fig. 4 for clarification. The quantities k_w and k_s

are functions of $\mathbf{t}_S \equiv (t_{S1}, t_{S2})$ and $\mathbf{t}_I \equiv (t_{I1}, t_{I2}, t_{I3}, t_{I4})$, and k_s has the periodicity $k_s(\mathbf{t}_S, \mathbf{t}_I) = k_s(\mathbf{t}_S, -\mathbf{t}_I) + 2\pi$.

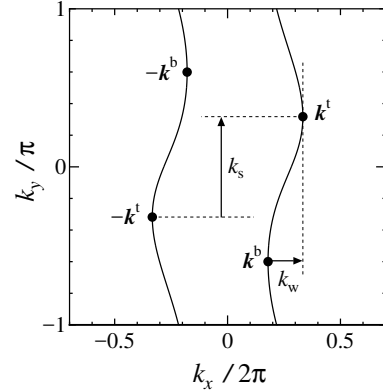


Fig. 4. Definitions of k_s and k_w . The black solid curves show the sheets of the Q1D open Fermi surface. The black closed circles show the top and bottom momenta $\pm \mathbf{k}^t$ and $\pm \mathbf{k}^b$, respectively. The elements k_x and k_y are plotted in the rectangular window for convenience; however, the angle between \mathbf{a} and \mathbf{b} is properly treated in the calculation.

4. Numerical Results

In this section, we examine the correlations between the optimal in-plane magnetic-field angle ϕ_0 and the structure of the Fermi surface and additionally investigate the maximum value of the magnitude of the upper critical field $H_{c2}(\phi_0)$. First, we examine the effects of each hopping integral, and then we examine the correlation between ϕ_0 and the shape of the Fermi surface.

4.1 Effect of staggered intra-chain hopping integrals

We examine the dependences of ϕ_0 and $h_c(\phi_0)$ on the ratio t_{S2}/t_{S1} of the two intra-chain hopping integrals. For $(\text{TMTSF})_2\text{ClO}_4$, this ratio deviates from unity because of the dimerization of TMTSF molecules. Figure 5 shows the numerical results, which imply that ϕ_0 and $h_c(\phi_0)$ are not substantially modified for small deviations realistic for conventional Q1D organic conductors. For example, it has been suggested in previous studies^{36,46)} that the deviation is 14–16% in $(\text{TMTSF})_2\text{ClO}_4$.

4.2 Dependence on inter-chain hopping integrals

The dependences of $h_c(\phi_0)$ and ϕ_0 on the inter-chain hopping integrals are much stronger than those on the intra-chain hopping integrals. Among them, the value of t_{I4} affects ϕ_0 and $h_c(\phi_0)$ most significantly. Two examples are shown in Fig. 6. As shown in the lower panel, ϕ_0 varies substantially when t_{I4} varies. The upper panel shows that $h_c(\phi_0)$ also strongly depends on t_{I4} . This tendency is emphasized when the other inter-chain hopping integrals are small. An example can be found by comparison between the black solid and red dashed curves in Fig. 6.

The dependence of ϕ_0 on the other inter-chain hopping integrals t_{I1} , t_{I2} , and t_{I3} is relatively weak, as shown in Fig. 7. In this figure, $h_c(\phi_0)$ significantly increases near $t_{I1} = -t_{I2}$, when $t_{I3} = t_{I4} = 0$ because the Fermi surface is flat at this point.

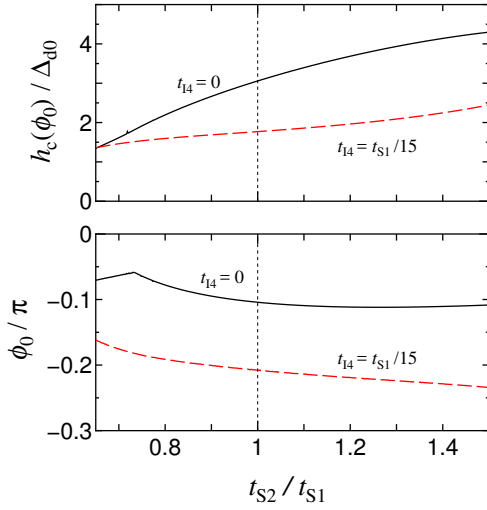


Fig. 5. t_{S2}/t_{S1} dependence of the optimal angle ϕ_0 (lower panel) and $h_c(\phi_0)$ (upper panel) for $(t_{11}, t_{12}, t_{13}) = (-1, -2, 2)t_{S1}/6$. The black solid and red dashed curves are the results for $t_{14} = 0$ and $t_{14} = t_{S1}/15$, respectively.

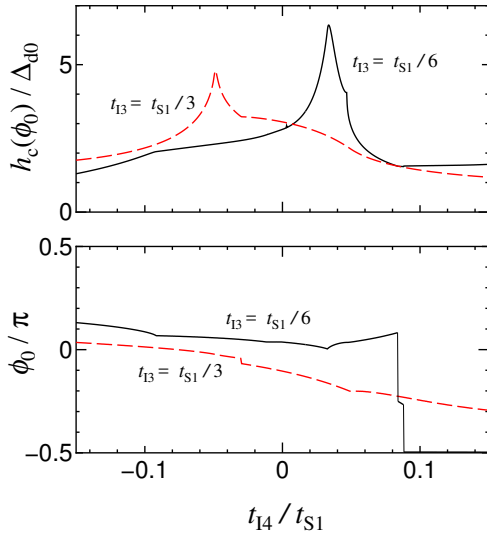


Fig. 6. t_{14} dependences of ϕ_0 and $h_c(\phi_0)$ when $t_{S1} = t_{S2}$, $t_{11} = -t_{S1}/6$, and $t_{12} = -t_{S1}/3$ are assumed. The black solid and red dashed curves are the results for $t_{13} = t_{S1}/6$ and $t_{13} = t_{S1}/3$, respectively.

For such a flat Fermi surface, however, the FFLO state is suppressed because the nesting instability to SDW or CDW is induced by the strong short-range repulsions, electron–lattice interactions, and lattice deformations, which exist in real materials.

In Figs. 6 and 7, ϕ_0 jumps at some values of inter-chain hopping integrals, and these jumps correspond to jumps of the nesting vector. Because the inter-chain hopping integrals vary with the applied pressure, the jumps of ϕ_0 may be observed in compounds with appropriate hopping integrals when the applied pressure increases.

The behaviors of ϕ_0 and $h_c(\phi_0)$ in wider ranges of the hopping integrals are shown in Fig. 8. In the left panels, ϕ_0 is small in the light-blue and light-green areas. When $t_{14} = 0$, such areas are large, especially where $h_c(\phi_0)$ is large (the dark-red area in the right panel). In the top-right panel, the curve of

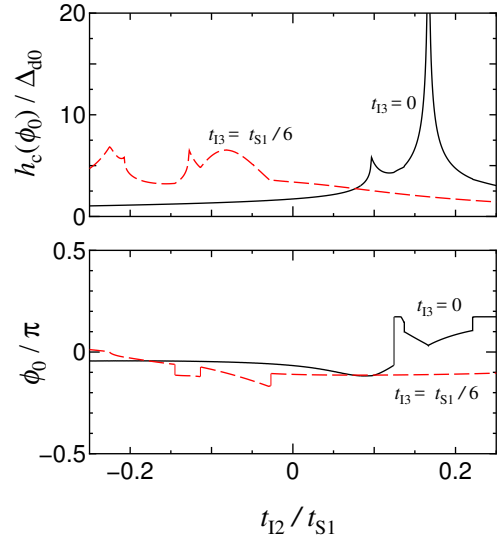


Fig. 7. Behaviors of ϕ_0 and $h_c(\phi_0)$ as functions of t_{12} when $t_{S1} = t_{S2}$, $t_{14} = 0$, and $t_{11} = -t_{S1}/6$. The black solid and red dashed curves show the results for $t_{13} = 0$ and $t_{13} = t_{S1}/6$, respectively.

$\phi_0 = 0$ (the dashed curve) runs through the dark-red area. This implies that the optimal direction, if the FFLO state is stabilized, tends to be parallel to the a -axis when $t_{14} = 0$. As t_{14} increases, however, the blue and green areas become darker where $h_c(\phi_0)$ is large. The curve of $\phi_0 = 0$ shifts, and the dark-red area moves away from the dashed curve. The dark-red areas in the right panels and the dark-blue or dark-green areas in the left panels occupy a larger common area for a larger t_{14} , which implies that the optimal direction approaches the b' -axis ($\phi_0 = \pm\pi/2$). The points marked by the closed circles represent the parameter sets P_{ave} , M_1 , and M_2 , which can be realistic for $(TMTSF)_2ClO_4$. These points are close to the boundaries on which $\phi_0 = \pm\pi/2$, and $h_c(\phi_0)$ is large at these points, as found in our previous letter.²⁶⁾

It is also found in the left panels in Fig. 8 that ϕ_0 can jump when the hopping parameters change, and such jumps correspond to the jumps in ϕ_0 found in Fig. 7. In particular, the jump occurs on some parts of the boundaries between the areas of $\phi_0 > 0$ and $\phi_0 < 0$.

4.3 Effect of Fermi-surface distortion on optimal in-plane magnetic-field direction

Next, we examine the correlation between the optimal angle ϕ_0 and the shape of the Fermi surface. (Note that h does not affect the shape of the Fermi surface drawn in the Brillouin zone, because h is much smaller than the hopping integrals.) To find the correlation, we examine a wider region of the inter-chain hopping integrals that is presented in Table I, where $t_{S2}/t_{S1} = 0.85$. In this region, we sample $\mathbf{t}_1 = (t_{11}, t_{12}, t_{13}, t_{14})$ using a $17 \times 17 \times 17 \times 17$ grid. We exclude \mathbf{t}_1 for which the warp of the Fermi surface is so large that $k_w > 0.2\pi$ or the Fermi surface is closed.

Figure 9 shows the correlation between the shear distortion of the Fermi surface quantified by k_s and the optimal field angle ϕ_0 . It is found that most points concentrate in the region $-0.01 \lesssim \phi_0/\pi \lesssim 0.1$, which implies that the optimal field direction is roughly parallel to the a -axis. Therefore, considering the fact that the orbital pair-breaking effect is weak

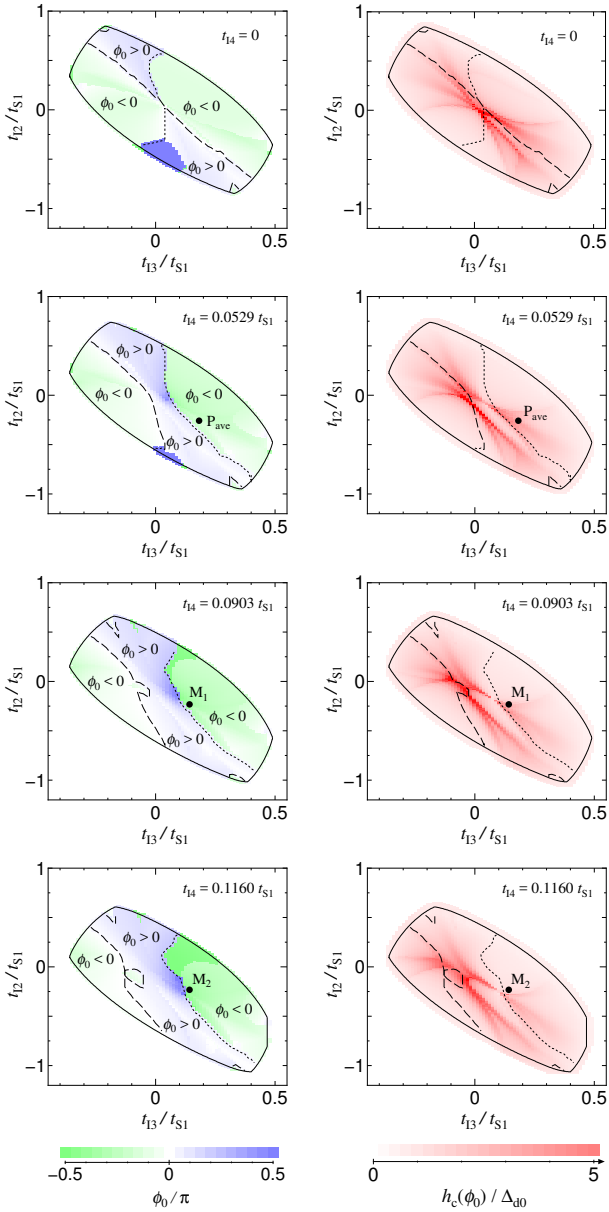


Fig. 8. Phase diagrams in the $t_{12}t_{13}$ planes for various values of t_{14} , where $t_{S2} = 0.85t_{S1}$ and $t_{11} = 0.129t_{S1}$ are assumed. The color scales are shown in the bottom panels. The solid curves are the boundaries of the areas in which the Fermi surface is open. The boundaries between the areas of $\phi_0 > 0$ and $\phi_0 < 0$ are presented by the dashed and dotted curves, on which, where ϕ_0 is continuous, $\phi_0 = 0$ and $\phi_0 = \pm\pi/2$, respectively. The parameter sets P_{ave} , M_1 , and M_2 have been defined in our previous letter.²⁶⁾

when $\phi_0 \approx 0$, we can predict that the FFLO state is stabilized most likely when the magnetic field is roughly parallel to the a-axis in Q1D systems with open Fermi surfaces. However, when the shear distortion of the Fermi surface is in the region $|k_s - \pi/2 \pm \pi| \lesssim 0.4\pi$, the optimal angle ϕ_0 can substantially deviate from 0. The parameter sets P_{ave} , M_1 , and M_2 are situated in this region, as presented by the violet closed squares in Fig. 9. As k_s increases in the region $|k_s - \pi/2 \pm \pi| \lesssim 0.4\pi$, ϕ_0 tends to increase from -0.42π to γ , although the correlation between ϕ_0 and k_s is weak. It is also found that the field directions nearly parallel to the open direction of the Q1D Fermi surface ($\gamma \lesssim \phi_0 < \pi/2$) cannot be the optimal direction. This implies that the FFLO vector, i.e., the nesting vector for the

FFLO state, cannot point in this direction.

Table I. Parameter regions and intervals in sampling parameter sets, for which the correlations between ϕ_0 and the shape of the Fermi surface are examined. We assume that $t_{S2}/t_{S1} = 0.85$.

Parameter	Region	Interval
t_{11}/t_{S1}	$[-0.8, 0.8]$	0.1
t_{12}/t_{S1}	$[-0.8, 0.8]$	0.1
t_{13}/t_{S1}	$[-0.4, 0.4]$	0.05
t_{14}/t_{S1}	$[-0.2, 0.2]$	0.025

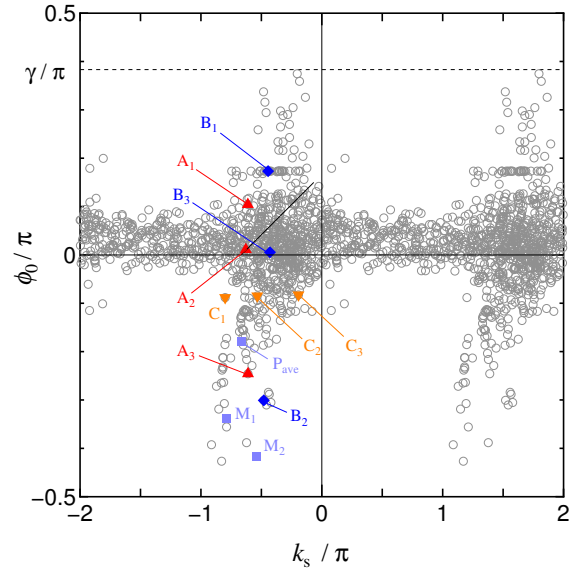


Fig. 9. Correlation between ϕ_0 and k_s , where the parameter sets are systematically sampled as explained in Table I and the text. Only the points for which $h_c > 3\Delta_{d0}$ are plotted. The short-dashed line represents $\phi_0 = \gamma = 69.0^\circ$. The violet closed squares represent the results for the parameter sets P_{ave} , M_1 , and M_2 . The red closed triangles, blue closed diamonds, and orange closed inverted triangles are the results of parameter sets named A_k , B_k , and C_k , respectively, which are explained in the text.

Let us focus on the parameter sets A_1 , A_2 , and A_3 , which result in the red closed triangles in Fig. 9. They give approximately the same values $(k_s, k_w) \approx (-0.6\pi, 0.08\pi)$, which implies that their Fermi surfaces have the same degrees of shear distortion and warp, and thus, as shown in Fig. 10, their shapes are similar. Despite this fact, the optimum angles ϕ_0 for A_1 , A_2 , and A_3 are quite different, as shown in Fig. 9, i.e., $\phi_0 = 0.104\pi$, 0.0111π , and -0.246π , respectively.

The parameter sets B_1 , B_2 , and B_3 , which result in the blue closed diamonds in Fig. 9, give another example in which the Fermi surfaces with approximately the same values $(k_s, k_w) \approx (-0.4\pi, 0.05\pi)$ yield quite different optimum angles: $\phi_0 = 0.173\pi$, 0.00559π , and -0.301π , respectively. For B_1 , B_2 , and B_3 , the shapes of the Fermi surfaces are shown in Fig. 10.

Conversely, Fermi surfaces with completely different shapes can yield the same optimum directions. The parameter sets C_1 , C_2 , and C_3 , which result in the orange closed

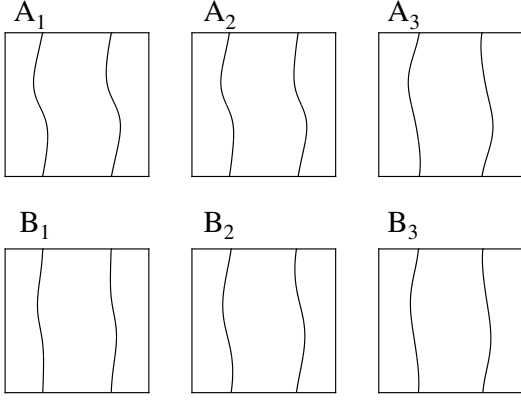


Fig. 10. Shapes of the Fermi surfaces for the parameter sets A_1 , A_2 , A_3 , B_1 , B_2 , and B_3 shown in Fig. 9.

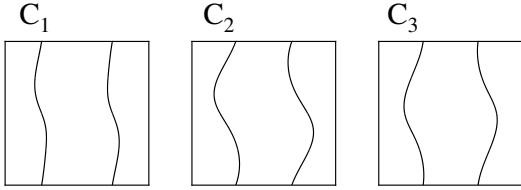


Fig. 11. Shapes of the Fermi surfaces for the parameter sets C_1 , C_2 , and C_3 shown in Fig. 9.

inverted triangles in Fig. 9, yield approximately the same optimum directions $\phi_0 \approx -0.08\pi$, whereas they give quite different shapes of the Fermi surfaces, as shown in Fig. 11.

These results for A_k , B_k , and C_k imply that, when $-0.8\pi \lesssim k_s \lesssim -0.2\pi$ and $1.2\pi \lesssim k_s \lesssim 1.8\pi$, although there is a weak tendency as mentioned above, the optimum direction cannot be predicted by simple consideration based on the shape of the Fermi surface.

Next, we examine the correlation between θ_s and ϕ_0 and its dependence on k_w , where θ_s is the shear angle defined by

$$\tan \theta_s = \frac{\mathbf{k}^t \cdot \hat{\mathbf{b}}'}{\mathbf{k}^t \cdot \hat{\mathbf{a}}}, \quad (6)$$

where $\hat{\mathbf{a}}$ and $\hat{\mathbf{b}}'$ are the unit vectors parallel to the a - and b' -axes, respectively. As depicted in Fig. 12, θ_s is the angle between the vector \mathbf{k}^t and the crystal a -axis in real space. Figure 13 shows that most points concentrate in the region $-0.02\pi \lesssim \phi_0 \lesssim 0.1\pi$, which means that the optimal field direction is roughly parallel to the a -axis. However, when the warp of the Fermi surface is small, as illustrated by the red open circles for $k_w < 0.13\pi$, while the shear distortion is moderate, i.e., for $-0.3 \lesssim \theta_s/\pi \lesssim -0.1$ or for $0.15 \lesssim \theta_s/\pi \lesssim 0.3$, the optimal angle ϕ_0 can substantially deviate from 0, exhibiting a tendency to increase from -0.42π to γ for increasing θ_s in these regions.

5. Summary and Discussion

We examined strongly Pauli-limited Q1D type-II superconductors using a model that has two intra-chain hopping integrals t_{S1} and t_{S2} and four inter-chain hopping integrals t_{I1} ,

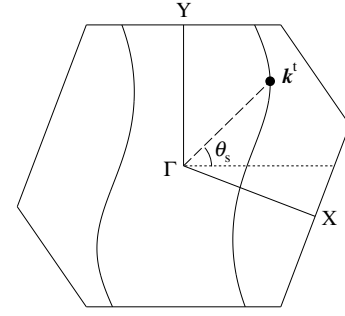


Fig. 12. Definition of θ_s [Eq. (6)]. The dotted line represents the direction of the a -axis.

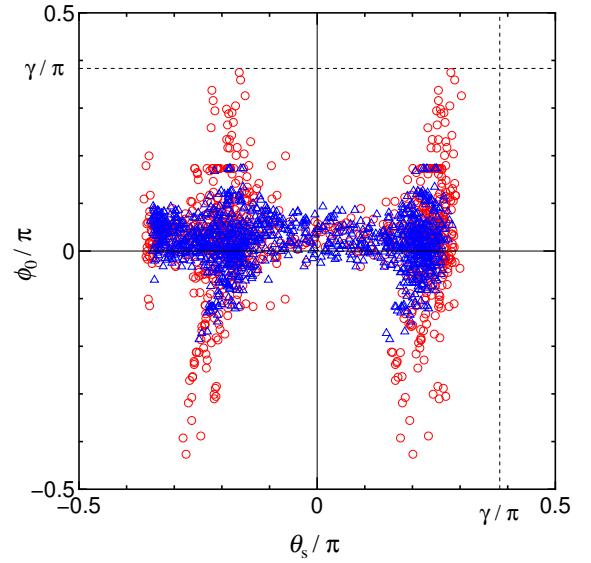


Fig. 13. Correlation between θ_s and ϕ_0 , where the parameter sets are systematically sampled as explained in Table I and the text. Only the points for which $h_c > 3\Delta_{d0}$ are plotted. The red open circles and blue open triangles show the points of $k_w < 0.13\pi$ and $0.2\pi > k_w > 0.13\pi$, respectively. The short-dashed straight lines represent $\phi_0 = \gamma$ and $\theta_s = \gamma$, where $\gamma = 69.0^\circ$.

t_{I2} , t_{I3} , and t_{I4} , as depicted in Fig. 2. We focused on the systems having an open Fermi surface that consists of two sheets of $k_x > 0$ and $k_x < 0$. Because the upper critical field is significantly enhanced for the in-plane magnetic field when $\phi \approx \pm\phi_0$, we examined the behaviors of ϕ_0 and $H_{c2}(\phi_0)$ that depend on the structure of the Fermi surface.

First, we examined the effect of the deviation of the intra-chain hopping integrals t_{S1} and t_{S2} , which is present in organic conductors such as $(\text{TMTSF})_2\text{ClO}_4$. It was found that this deviation does not have a major effect on ϕ_0 and $H_{c2}(\phi_0)$. Next, we examined the effects of changes in the inter-chain hopping integrals, which can be induced by applied and chemical pressures. It was found that they change both ϕ_0 and $H_{c2}(\phi_0)$ significantly. In particular, jumps in ϕ_0 were predicted, and they would be interesting phenomena if observed. Among the inter-chain hopping integrals, t_{I4} has the most significant effect on ϕ_0 . The optimal in-plane magnetic-field direction approaches the b' -axis when t_{I4} increases. If ϕ_0 as observed in $(\text{TMTSF})_2\text{ClO}_4$ is to be realized, t_{I4} must be sufficiently large.

We also examined the correlation between ϕ_0 and the shape

of the Fermi surface. We defined k_w to quantify the warp of each sheet, and we defined k_s and θ_s to quantify the shear distortion between the two sheets. Although the correlation is weak, we found some tendencies: in most cases, the optimal field direction is roughly parallel to the a-axis and tends to be slightly rotated toward the b-axis ($-0.01 \lesssim \phi_0/\pi \lesssim 0.1$). This asymmetry with respect to $\phi_0 = 0$ is due to the fact that $\gamma < \pi/2$. In addition, the orbital pair-breaking effect, when incorporated, is weakest for a magnetic field parallel to the most conductive chain. Therefore, the present result implies that in most cases, the FFLO state is stabilized for magnetic-field directions roughly parallel to the a-axis. In contrast, when the warp is small while the shear distortion is moderate, ϕ_0 can take any value except for the values between the b- and b'-axes. In terms of k_w and k_s , this condition is expressed as $k_w \lesssim 0.13\pi$ and $|k_s - \pi/2 \pm \pi| \lesssim 0.4\pi$. When these conditions are satisfied, Fermi surfaces with similar shapes can result in quite different values of ϕ_0 , and conversely, Fermi surfaces with entirely different shapes can result in the same value of ϕ_0 .

We assumed d-wave pairing in the present calculation; however, this assumption does not affect the behavior of ϕ_0 significantly. We confirmed by explicit calculations that the value of ϕ_0 is not strongly affected by the difference in the pairing symmetry, unless the node of the order parameter is close to the nesting point on the Fermi surface. We also confirmed that for the same reason, the order-parameter mixing⁴⁷⁻⁴⁹ does not affect the value of ϕ_0 , although it affects the magnitude of the upper critical field and the tricritical temperature.

The present result does not explain the magnetic-field and temperature dependences of the optimal angle ϕ_0 observed in (TMTSF)₂ClO₄. This discrepancy may be resolved if the orbital pair-breaking effect is incorporated: if vortex states with higher Landau-level indexes occur, the order-parameter modulation in the direction perpendicular to the magnetic field is practically a perpendicular component of the FFLO vector \mathbf{q} ,^{4,5,21,29} which implies that $\phi_{\mathbf{q}} \neq \phi$. Therefore, the orbital pair-breaking effect may cause the temperature dependence of ϕ_0 .

The orbital pair-breaking effect also strongly reduces the magnitude of the upper critical field. However, since the upper critical fields near $\phi = \pm\phi_0$ are very large in the above result, it is likely that they would exceed the Pauli paramagnetic limit for such field directions, even if it is reduced by the orbital pair-breaking effect.

In conclusion, the dependence of the optimal in-plane magnetic-field direction on the structure of the Fermi surface was clarified in Q1D systems with open Fermi surfaces. We expect that the results summarized above can be useful for future studies on the FFLO state in Q1D conductors.

Acknowledgments

The authors would like to thank S. Yonezawa and K. Kishigi for useful discussions.

1) P. Fulde and R. A. Ferrell, Phys. Rev. **135**, A550 (1964).

2) A. I. Larkin and Yu. N. Ovchinnikov, Zh. Eksp. Teor. Fiz. **47**, 1136 (1964); translation: Sov. Phys. JETP **20**, 762 (1965).

- 3) R. Casalbuoni and G. Nardulli, Rev. Mod. Phys. **76**, 263 (2004).
- 4) Y. Matsuda and H. Shimahara, J. Phys. Soc. Jpn. **76**, 051005 (2007).
- 5) H. Shimahara, in *The Physics of Organic Superconductors and Conductors*, ed. A.G. Lebed (Springer, Berlin, 2008), p. 687.
- 6) H. Shimahara, Phys. Rev. B **50**, 12760 (1994).
- 7) H. Shimahara, J. Phys. Soc. Jpn. **66**, 541 (1997).
- 8) J. Singleton, J. A. Symington, M.-S. Nam, A. Ardavan, M. Kurmoo, and P. Day, J. Phys. Condens. Matter **12**, L641 (2000).
- 9) J. A. Symington, J. Singleton, M.-S. Nam, A. Ardavan, M. Kurmoo, and P. Day, Physica B **294-295**, 418 (2001).
- 10) R. Lortz, Y. Wang, A. Demuer, P. H. M. Böttger, B. Bergk, G. Zwignagl, Y. Nakazawa, and J. Wosnitzer, Phys. Rev. Lett. **99**, 187002 (2007).
- 11) J. A. Wright, E. Green, P. Kuhns, A. Reyes, J. Brooks, J. Schlueter, R. Kato, H. Yamamoto, M. Kobayashi, and S. E. Brown, Phys. Rev. Lett. **107**, 087002 (2011).
- 12) I. J. Lee, M. J. Naughton, G. M. Danner, and P. M. Chaikin, Phys. Rev. Lett. **78**, 3555 (1997).
- 13) S. Yonezawa, S. Kusaba, Y. Maeno, P. Auban-Senzier, C. Pasquier, K. Bechgaard, and D. Jerome, Phys. Rev. Lett. **100**, 117002 (2008).
- 14) S. Yonezawa, S. Kusaba, Y. Maeno, P. Auban-Senzier, C. Pasquier, and D. Jerome, J. Phys. Soc. Jpn. **77**, 054712 (2008).
- 15) S. Yonezawa, Y. Maeno, K. Bechgaard, and D. Jérôme, Phys. Rev. B **85**, 140502(R) (2012).
- 16) S. Uji, K. Kodama, K. Sugii, T. Terashima, Y. Takahide, N. Kurita, S. Tsuchiya, M. Kimata, A. Kobayashi, B. Zhou, and H. Kobayashi, Phys. Rev. B **85**, 174530 (2012).
- 17) M. Houzet, A. Buzdin, L. Bulaevskii, and M. Maley, Phys. Rev. Lett. **88**, 227001 (2002).
- 18) H. Shimahara, J. Phys. Soc. Jpn. **71**, 1644 (2002).
- 19) M.A. Tanatar, T. Ishiguro, H. Tanaka, and H. Kobayashi, Phys. Rev. B **66**, 134503 (2002).
- 20) L. W. Gruenberg and L. Gunther, Phys. Rev. Lett. **16**, 996 (1966).
- 21) H. Shimahara and D. Rainer, J. Phys. Soc. Jpn. **66**, 3591 (1997).
- 22) H. Shimahara, J. Supercond. **12**, 469 (1999).
- 23) In this argument, we assume that the orbital pair-breaking effect is weak; however, for the field-direction dependence to emerge, the presence of the orbital pair-breaking effect is necessary. When the orbital pair-breaking effect is negligible, the field-direction dependence vanishes.
- 24) The FFLO state can have two \mathbf{q} values²⁾ or more than two \mathbf{q} values.^{5,50} However, the second-order transition point can be examined where a single \mathbf{q} is assumed.
- 25) N. Miyawaki and H. Shimahara, J. Phys. Soc. Jpn. **83**, 024703 (2014).
- 26) K. Itahashi and H. Shimahara, J. Phys. Soc. Jpn. **87**, 083701 (2018).
- 27) A. G. Lebed, Phys. Rev. Lett. **107**, 087004 (2011).
- 28) M. D. Croitoru, M. Houzet, and A. I. Buzdin, Phys. Rev. Lett. **108**, 207005 (2012).
- 29) H. Shimahara, Phys. Rev. B **80**, 214512 (2009).
- 30) When the orbital pair-breaking effect is extremely weak, the states expressed by the Abrikosov function with a higher Landau-level index can be stable.^{21,29} The spatial modulation in those functions is reduced to that of the FFLO state in the limit of weak orbital effect. Hence, when the orbital effect is extremely weak, practically speaking, the direction of the FFLO oscillation is not necessarily parallel to the direction of the magnetic field.^{5,29}
- 31) H. Shimahara, J. Phys. Soc. Jpn. **68**, 3069 (1999).
- 32) H. Shimahara and K. Moriwake, J. Phys. Soc. Jpn. **71**, 1234 (2002); H. Shimahara and S. Hata, Phys. Rev. B **62**, 14541 (2000).
- 33) K. Machida and H. Nakanishi, Phys. Rev. B **30**, 122 (1984).
- 34) Y. Suzumura and K. Ishino, Prog. Theor. Phys. **70**, 654 (1983).
- 35) Strictly speaking, $n = 4$ can hold at cusps even in the present shear-distorted Q1D systems. Furthermore, even when $n = 2$, the cusp can occur when the Fermi surfaces touches on two lines (i.e., two points in the k_x - k_y plane) for an appropriate magnetic-field direction.
- 36) D. Le Pévelén, J. Gaultier, Y. Barrans, D. Chasseau, F. Castet, and L. Ducasse, Eur. Phys. J. B **19**, 363 (2001).
- 37) K. Kishigi and Y. Hasegawa, Phys. Rev. B **94**, 085405 (2016).
- 38) N. Miyawaki and H. Shimahara, J. Phys.: Conf. Ser. **702**, 012002 (2016).
- 39) H. Shimahara, Phys. Rev. B **61**, R14936 (2000).
- 40) For convenience, we repeat the result of our previous letter.²⁶⁾ The FFLO vector \mathbf{q} is taken into the theory through $\varphi_{\mathbf{q}} = \arctan(q_y/q_x)$ and $q_1 = (q_x^2 + q_y^2)^{1/2}$, where $q_x = \mathbf{q} \cdot \mathbf{a}$ and $q_y = \mathbf{q} \cdot \mathbf{b}$. The true magnitude $q = |\mathbf{q}|$ and the angle $\phi_{\mathbf{q}}$ between \mathbf{q} and the a-axis are related to

$\varphi_{\mathbf{q}}$ and q_1 as

$$q \cos \phi_{\mathbf{q}} = \mathbf{q} \cdot \hat{\mathbf{a}} = \frac{q_1}{a} \cos \varphi_{\mathbf{q}},$$

$$q \sin \phi_{\mathbf{q}} = \mathbf{q} \cdot \hat{\mathbf{b}}' = \frac{q_1}{a} \left(\frac{a}{b} \frac{\sin \varphi_{\mathbf{q}}}{\sin \gamma} - \frac{\cos \varphi_{\mathbf{q}}}{\tan \gamma} \right),$$

where $\hat{\mathbf{a}} \equiv \mathbf{a}/|\mathbf{a}|$ and $\hat{\mathbf{b}}'$ denotes the unit vector perpendicular to \mathbf{a} .

- 41) S. Kusaba, S. Yonezawa, Y. Maeno, P. Auban-Senzier, C. Pasquier, K. Bechgaard, and D. Jérôme, *Solid State Sci.* **10**, 1768 (2008).
- 42) Equation (3) should be the dispersion relation of holes in the application to organic superconductors.
- 43) H. Shimahara, *J. Phys. Soc. Jpn.* **58**, 1735 (1989).
- 44) Y. Hasegawa and H. Fukuyama, *J. Phys. Soc. Jpn.* **56**, 877 (1987).
- 45) M. Takigawa, H. Yasuoka, and G. Saito, *J. Phys. Soc. Jpn.* **56**, 873 (1987).
- 46) P. Alemany, J.-P. Pouget, and E. Canadell, *Phys. Rev. B* **89**, 155124 (2014).
- 47) S. Matsuo, H. Shimahara, and K. Nagai, *J. Phys. Soc. Jpn.* **63**, 2499 (1994).
- 48) H. Shimahara, *Phys. Rev. B* **62**, 3524 (2000).
- 49) H. Shimahara, *J. Phys. Soc. Jpn.* **69**, 1966 (2000).
- 50) H. Shimahara, *J. Phys. Soc. Jpn.* **67**, 736 (1998).